ESAIM: PROCEEDINGS, December 2012, Vol. 38, p. 361-375
F. Coquel, M. Gutnic, P. Helluy, F. Lagoutière, C. Rohde, N. Seguin, Editors

CURRENT IDENTIFICATION IN VACUUM CIRCUIT BREAKERS AS A LEAST SQUARES PROBLEM *

Luca Ghezzi[1] and Francesca Rapetti[2]

Abstract. In this work, a magnetostatic inverse problem is solved, in order to reconstruct the electric current distribution inside high voltage, vacuum circuit breakers from measurements of the outside magnetic field. The (rectangular) final algebraic linear system is solved in the least square sense, by involving a regularized singular value decomposition of the system matrix. An approximated distribution of the electric current is thus returned, without the theoretical problem which is encountered with optical methods of matching light to temperature and finally to current density. The feasibility is justified from the computational point of view as the (industrial) goal is to evaluate whether, or to what extent in terms of accuracy, a given experimental set-up (number and noise level of sensors) is adequate to work as a "magnetic camera" for a given circuit breaker.

Résumé. Dans cet article, on résout un problème inverse magnétostatique pour déterminer la distribution du courant électrique dans le vide d'un disjoncteur à haute tension à partir des mesures du champ magnétique extérieur. Le système algébrique (rectangulaire) final est résolu au sens des moindres carrés en faisant appel à une décomposition en valeurs singulières regularisée de la matrice du système. On obtient ainsi une approximation de la distribution du courant électrique sans le problème théorique propre des méthodes optiques qui est celui de relier la lumière à la température et donc à la densité du courant. La faisabilité est justifiée d'un point de vue numérique car le but (industriel) est d'évaluer si, ou à quelle précision, un dispositif expérimental donné (nombre et seuil limite de bruit des senseurs) peut travailler comme une "caméra magnétique" pour un certain disjoncteur.

Introduction

Circuit breakers are protection devices which are inserted into electric networks in order to clear faults such as short circuits and overloads. Under faulty and possibly dangerous conditions, circuit breakers are operated in such a way to break the electric current flow by opening two contacting conductors, thus interrupting the electric continuity of the line. The technology adopted in circuit breakers, along with the size, depends on their rating, ranging from small devices that protect an individual household appliance up to large switchgear designed to protect high voltage circuits or power generators.

Whenever a current is interrupted, an electric arc is generated. This arc must be contained, cooled, and extinguished in a controlled way, so that the gap between the contacts can again withstand the voltage in the circuit. The medium in which the arc forms depends on the circuit breaker and may be vacuum, air, insulating gas (SF_6, CO_2), or even oil in old times. A common aspect is the crucial role played by plasma dynamics with

* *This project was supported by the grant* Mortar Elements for Industrial Devices (MEID) *of the program* Projets Exploratoires PluridisciplinaireS (PEPS) *in the theme* Mathematics in Industry (MI) *funded by the CNRS-INSMI Institute.*

[1] ABB S.p.A., Via dell'Industria 18, 20010 Vittuone, Italy

[2] Laboratoire J.A. Dieudonné, Université de Nice Sophia-Antipolis, Parc Valrose, 06108 Nice cédex 02, France

reference to the final interruption outcome, which makes the arc the core technological issue in circuit breaker engineering; see [3]. The knowledge of electric current distribution in space and time, during an interruption process, helps understanding the complex physical behavior of the electric arc and allows technicians to evaluate the effect of design choices.

Standard experimental techniques for arc diagnostic are of optical nature, including imaging by means of CCD cameras or fiber optics. Despite being well assessed and appreciated, optical methods are deemed invasive and to some extent perturbative of the real physical conditions, since observations screens of different materials are produced, or holes for hosting fibers are drilled in the sidewalls of otherwise opaque circuit breakers. The preparation of the experimental setup is also time consuming and not easy, especially in the case of vacuum circuit breakers, owing to the need for preserving gastightness and preventing the surrounding atmosphere from penetrating inside the breaker. To prevent from saturation of the filming device, optical methods require suitable and non trivial filtering techniques, which may strongly affect the reliability of the collected data; see [7]. The translation of an observed light pattern into a temperature pattern and, finally, into an electric current density pattern is an issue itself, whose complexity is increased by the progressive blindening of the optical tool, produced by the soot and debris released during arcing.

An alternative experimental method is the reconstruction of the current distribution from measurements of the magnetic field. An inverse problem needs to be solved, allowing the determination of the causes, i.e., electric currents inside the circuit breaker, starting from the effects, i.e., the magnetic field outside the circuit breaker.

In this work, we analyze from the numerical point of view the magnetic inverse problem to solve for the current reconstruction in the circuit breaker chamber. In the linear algebra framework, we are concerned with the least squares solution of a system of equations where the system matrix is generally rectangular (more unknowns than equations or viceversa) and frequently rank deficient. We note that the numerical solution of linear least-squares problems is a key computational task in science and engineering. Effective algorithms have been developed for the linear least-squares problems in which the underlying matrices have full rank and are well-conditioned. However, there are few efficient and robust approaches to solving the linear least-squares problem in which the underlying matrices are rank-deficient and sparse. The method to solve the considered circuit breaker problem is based on a classical Single Value Decomposition (SVD) of the system matrix [5] combined with a particular Smith normal form (SMF) algorithm [8, 9] for the divergence-free constraint on the current density.

1. Continuous direct problem description

The current identification method is applied to a Vacuum Circuit Breaker (VCB). A simplified geometry of a typical VCB is shown in Fig. 1. The VCB is constituted by two copper terminals, occupying domains Ω_1 and Ω_2. The shape of each of the two conductors is approximated by the union of circular disc and a slender cylinder, the latter being the connection of the VCB to the rest of the electric network. When the breaker is in closed position, the two discs contact one against the other. As soon as the contacts are opened, a cylindrical gap is formed, occupying the domain Ω_p. Such a gap hosts the plasma phase, where electric current density has to be identified.

We denote by $\Omega_c := \Omega_1 \cup \Omega_p \cup \Omega_2$ the conductive or potentially conductive portion of the problem at hand, including into this denomination also those region of Ω_p characterized by a low electrical conductivity. The surrounding domain Ω_a is occupied by external air, and has to be considered as insulating, since electric current has no way to leave Ω_c. Finally we introduce the domain $\Omega := \Omega_c \cup \Omega_a$. We may assume, with no loss of generality as regards the technical application, that both Ω_c and Ω are simply connected.

In absence of (linear or nonlinear) ferromagnetic inclusions and charge accumulation, the direct problem consists in finding the magnetic field $\mathbf{H}$ which is related in Ω to the conduction current density $\mathbf{J}$ and to the magnetic flux density $\mathbf{B}$ by

$$\nabla \times \mathbf{H} = \mathbf{J}, \quad \nabla \cdot \mathbf{B} = 0, \quad \mathbf{B} = \mu \mathbf{H}, \quad \nabla \cdot \mathbf{J} = 0, \tag{1}$$

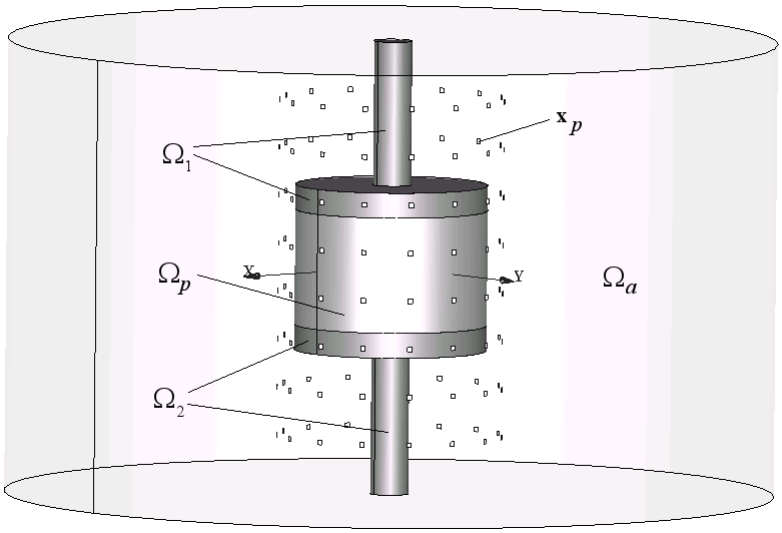

FIGURE 1. Geometry of a VCB.

where $\mu = \mu_0$ since we consider "vacuum" circuit breakers. We remark that even in presence of para- or dia-magnetic media in the breaker, the assumption $\mu = \mu_0$ is still considered at the engineering level since the highest errors are related to measurements. Problem (1) is closed by suitable boundary conditions related to the total current I flowing through the VCB. Indeed, let $\partial\Omega_c^1$ (resp., $\partial\Omega_c^2$) be the "in" (resp., "out") terminal, i.e., the portion of the boundary $\partial\Omega_c$ of the conducting domain Ω_c where electric current $I_1 = -I$ (resp., $I_2 = +I$) enters into (resp., exits from) Ω_c. We may always assume, up to swapping the names of domains, that $\partial\Omega_c^1$ (resp., $\partial\Omega_c^2$) be a portion of the boundary $\partial\Omega_1$ (resp., $\partial\Omega_2$) of Ω_1 (resp., Ω_2). Let A_1 (resp., A_2) be the surface area of $\partial\Omega_c^1$ (resp., $\partial\Omega_c^2$). Let $\partial\Omega_c^0 = \partial\Omega_c \backslash (\partial\Omega_c^1 \cup \partial\Omega_c^2)$ be the lateral skin of Ω_c, that is, the interface between Ω_c and Ω_a. Since the latter is insulant, no cross flow of electric current is possible and $\mathbf{J}$ is tangent to $\partial\Omega_c^0$, thus

$$\int_{\partial\Omega_c^i} \mathbf{J} \cdot \mathbf{n} = I_i, \qquad i \in \{0, 1, 2\}, \tag{2}$$

where $I_0 := 0$.

2. Discrete inverse problem description

In order to state the discrete inverse problem, we firstly introduce $\mathcal{T}$, a conforming discretization of the domain $\bar{\Omega}$, consisting in oriented cells, that are simplices in the present case. Let S_n be the set of n-simplices of the complex $\mathcal{T} = \cup_{n=0}^3 S_n$. We term $\mathcal{N} = S_0$, $\mathcal{E} = S_1$, $\mathcal{F} = S_2$ and $\mathcal{C} = S_3$ the node, edge, face and cell sets, respectively, of the complex $\mathcal{T}$. Then $|\mathcal{N}|$, $|\mathcal{E}|$, $|\mathcal{F}|$ and $|\mathcal{C}|$ are the number of nodes, of edges, of faces and of cells, respectively. Additionally, let $\mathcal{T}_1$, $\mathcal{T}_2$, $\mathcal{T}_p$, and $\mathcal{T}_c$ be the sub-complexes of $\mathcal{T}$ discretizing Ω_1, Ω_2, Ω_p, and Ω_c, respectively. Union and intersection relations, such as $\mathcal{T}_1 \cup \mathcal{T}_p \cup \mathcal{T}_2 = \mathcal{T}_c$, are naturally inherited by analogous relations holding in the exact, continuous frame. Finally, let $|\mathcal{N}_p|$, $|\mathcal{E}_p|$, $|\mathcal{F}_p|$ and $|\mathcal{C}_p|$ be the number of nodes, of edges, of faces and of cells of $\mathcal{T}_p$, respectively. Analogous definitions are assumed for the other sub-complexes.

Experimental or synthetic measures of the magnetic field intensity H are available in a collection $\{\mathbf{x}_p\}_{p=1}^{|\mathcal{P}|}$ of points $\mathbf{x}_p \in \Omega_a$, $p \in \{1, \ldots, |\mathcal{P}|\}$, where magnetic field sensors are located. These points $\mathbf{x}_p$ do not necessarily coincide with nodes of the mesh $\mathcal{T}$. Even though most sensors exploit some physical phenomenon in which only a directional component of the magnetic field vector is involved, we assume without loss of generality that

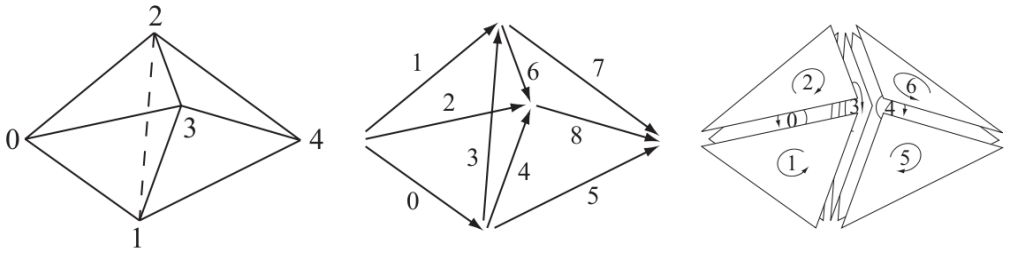

FIGURE 2. A simple mesh of two outwardly oriented simplices. The associated data structure includes the set of nodes $\mathcal{N} = \{0, 1, 2, 3, 4\}$, the set of (internally) oriented edges $\mathcal{E} = \{\ \{0,1\}, \{0,2\}, \{0,3\}, \{1,2\}, \{1,3\}, \{1,4\}, \{2,3\}, \{2,4\}, \{3,4\}\ \}$, the set of oriented facets $\mathcal{F} = \{\ \{0,1,2\}, \{0,1,3\}, \{0,2,3\}, \{1,2,3\}, \{1,2,4\}, \{1,3,4\}, \{2,3,4\}\ \}$ and the set of oriented tetrahedra $\mathcal{T} = \{\ \{0,1,2,3\}, \{1,2,3,4\}\ \}$. In this case, D is a 2×7 integer matrix with first line equal to $(-1, 1, -1, 1, 0, 0, 0)$ and second line $(0, 0, 0, -1, 1, -1, 1)$.

each probe senses the whole magnetic field vector; the latter condition may always be obtained, albeit in a somewhat approximated way, by locating three directional sensors very close together, in a neighborhood of the same point, and aligned along three independent directions. We denote by $|\mathcal{P}|$ the number of sensors available, so that $3|\mathcal{P}|$ is the number of measures. We thus introduce a vector $\mathbf{h}$ of size $3\,|\mathcal{P}|$ to collect the vectors $\mathbf{H}_p$, that are the measures of the field $\mathbf{H}$ associated to the points $\mathbf{x}_p$. We denotes by $\mathbf{j}$ the vector containing the degrees of freedom of $\mathbf{J}$ over the mesh $\mathcal{T}$, that are the values of the electric density fluxes across the $|\mathcal{F}|$ mesh faces. The inverse discrete algebraic counterpart of problem (1) reads: find $\mathbf{j}$ such that

$$D\mathbf{j} = \mathbf{0} \qquad \text{and} \qquad L\mathbf{j} = \mathbf{h}, \tag{3}$$

where D is the face-to-volume incidence matrix and L a linear discrete analogue of the Biot-Savart operator [1]. Note that, in typical industrial applications, $|\mathcal{F}| \gg 3|\mathcal{P}|$.

The first equation in problem (3) represents the discrete form of the divergence free constraint on the current density $\mathbf{J}$. The involved face-to-volume incidence matrix D is a $|\mathcal{C}|$ by $|\mathcal{F}|$ integer matrix with entries $D_{cf} \in \{0, 1, -1\}$, where $|\mathcal{C}|$ (resp. $|\mathcal{F}|$) is the number of cells (resp. faces) in the mesh $\mathcal{T}$. In detail, $D_{cf} = 0$ if f is not a face of the cell c. Otherwise, $D_{cf} = +1$ (resp. -1) if f is a face of c and its internal (for example counter-clockwise) orientation agrees (resp., disagrees) with the face orientation induced by the outward orientation of c on f; see Fig. 2.

Let $n := \dim \ker D$ be the dimension of the null space of D and $N \in \mathbb{R}^{|\mathcal{F}| \times n}$ be a matrix whose columns form a basis for $\ker D$. Since $DN\mathbf{z} = \mathbf{0}$, $\forall \mathbf{z} \in \mathbb{R}^{|\mathcal{F}|}$, the expression

$$\mathbf{j} = N\mathbf{z} \tag{4}$$

originates a generic divergence free current density distribution. Plugging (4) into (3), one gets the linear system to solve, namely find $\mathbf{z} \in \mathbb{R}^{|\mathcal{F}|}$ such that

$$LN\mathbf{z} = \mathbf{h}. \tag{5}$$

Despite the divergence free constraint allows eliminating a number of unknowns, the algebraic system (5) on the free unknowns typically remains underdetermined. The matrix N can be computed relying on the Smith normal form of D as described in the next section.

3. Integer QR factorization with column pivoting to construct N

Let us consider a matrix $A \in \mathbb{R}^{n \times m}$ with n rows and m columns, whose nullspace is described by the columns of a matrix N with $N \neq 0$. Practical methods to compute N are based on either the Single Value Decomposition

(SVD) of A or on the QR factorization of A with column pivoting, a method proposed by Golub in the mid-sixties [5]. The second method is much cheaper than the SVD and consists in using a column pivoting strategy to determine a permutation matrix P such that $AP = QR$ with $Q \in \mathbb{R}^{n\times n}$ satisfying $Q^\top Q = I_n$ and the upper triangular matrix R is partitioned as

$$R = \begin{pmatrix} R_{11} & R_{12} \\ 0 & R_{22} \end{pmatrix}$$

where $R_{11} \in \mathbb{R}^{r\times r}$ and R_{22} is small in norm. Let us assume $\sigma_1 \geq \sigma_2 \geq ... \geq \sigma_n \geq 0$, where σ_i are the singular values of A. Mathematically, in terms of singular values, we say that A has rank r if and only if $\sigma_r > 0$ and $\sigma_{r+1} = 0$. However, computationally, we may have σ_{r+1} not exactly equal to zero but $\sigma_{r+1} = O(\nu)$, where ν is the machine precision. If $\sigma_r \gg \sigma_{r+1}$, we say that A has numerical rank r. Equivalently, if, say, $||R_{22}||_2 = O(\nu)$, it can be proved that $\sigma_{r+1} \leq ||R_{22}||_2$. Thus we conclude that the original matrix A is guaranteed to have *at most* numerical rank r, that is, rank r up to the precision ν. The QR factorization of AP, where P is a permutation matrix chosen to yield a "small" R_{22}, is referred to as the Rank-Revealing QR (RRQR) factorization of A.

With both SVD and RRQR decompositions, the matrix A can be factorized as

$$A = U\Sigma V^\top, \tag{6}$$

where $U \in \mathbb{R}^{n\times n}$ and $V \in \mathbb{R}^{m\times m}$ are orthogonal matrices and $\Sigma \in \mathbb{R}^{n\times m}$. Being orthogonal, the rows as well the columns of U and V span $\mathbb{R}^n$ and $\mathbb{R}^m$, respectively. All of the non-zero entries of Σ are on the main diagonal and we suppose that these entries are ordered in such a way that the first r are non-null, while the remaining $p-r$ are null, with $p := \min\{m, n\}$. This is always possible by means of a suitable permutation of the rows and columns of A which will be memorized in the matrices U and V. In short, the following structure holds:

$$\Sigma = \begin{bmatrix} d_1 & \dots & 0 & 0 & \dots & 0 \\ \vdots & \ddots & \vdots & \vdots & \ddots & \vdots \\ 0 & \dots & d_r & 0 & \dots & 0 \\ 0 & \dots & 0 & 0 & \dots & 0 \\ \vdots & \ddots & \vdots & \vdots & \ddots & \vdots \\ 0 & \dots & 0 & 0 & \dots & 0 \end{bmatrix}. \tag{7}$$

The nullspace of A is contained in V:
The nullspace (or kernel) of matrix A is a vector subspace of $\mathbb{R}^m$ of those vectors $\mathbf{x}$ such that $A\,\mathbf{x} = \mathbf{0}$. Owing to the factorization (6), with U invertible, the condition for $\mathbf{x}$ to be in the nullspace of A may be rewritten as

$$\Sigma V^\top \mathbf{x} = \mathbf{0}. \tag{8}$$

Let us expand explicitly the above product and write

$$\mathbf{y} := \Sigma V^\top \mathbf{x} = \begin{bmatrix} d_1 \mathbf{v}_1^\top \mathbf{x} \\ \vdots \\ d_r \mathbf{v}_r^\top \mathbf{x} \\ 0 \\ \vdots \\ 0 \end{bmatrix} \in \mathbb{R}^n. \tag{9}$$

The condition that the newly introduced vector $\mathbf{y}$ must be null implies $d_i \mathbf{v}_i^\top \mathbf{x} = 0$, $i \in \{1, \dots, r\}$. Since $d_i \neq 0$, $i \in \{1, \dots, r\}$, by hypothesis, this implies $\mathbf{v}_i^\top \mathbf{x} = 0$, $i \in \{1, \dots, r\}$. In short, $\mathbf{x} \perp < \mathbf{v}_1, \dots, \mathbf{v}_r >$, i.e., $\mathbf{x}$ must be orthogonal to the subspace spanned by the first r columns of V. Therefore, $\mathbf{x} \in < \mathbf{v}_{r+1}, \dots, \mathbf{v}_n >$, i.e.,

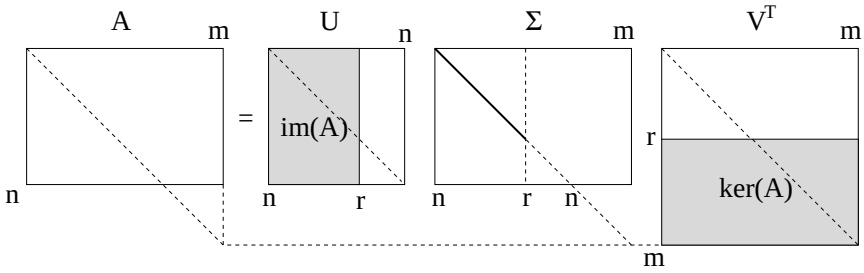

FIGURE 3. Visual sketch of the factorization (6), revealing the nullspace $\ker A$ (spanned by the rows in the gray part of matrix $V^\top$) and the range $\mathrm{im}A$ (spanned by the columns in the gray part of matrix U); the main diagonal of each matrix is shown as a guide to visualize the matrix size; the bold part of the main diagonal of Σ contains the only non-null entries of such a matrix.

$\mathbf{x}$ must lie in the orthogonal complement of $< \mathbf{v}_1, \ldots, \mathbf{v}_r >$ in $\mathbb{R}^m$, which is the subspace spanned by the last $m - r$ columns of V. We thus have that the last $m - r$ columns of V span the nullspace of A.

The range of A is contained in U:
The range of A is the subspace of $\mathbb{R}^n$ generated by those vectors of the form $A\mathbf{x}$ with $\mathbf{x} \in \mathbb{R}^m$. We remind that $A\,\mathbf{x} = U\,\mathbf{y}$. The i-th component of the generic element of the range reads

$$(A\,\mathbf{x})_i = \sum_{j=1}^{n} U_{ij} y_j = \sum_{j=1}^{r} U_{ij} y_j + \sum_{j=r+1}^{n} U_{ij} \cdot 0 = \sum_{j=1}^{r} U_{ij} y_j, \tag{10}$$

where the last passage holds because the last $n-r$ entries of $\mathbf{y}$ are zero by (9). Therefore, the last $n-r$ columns of U do not contribute to give $A\,\mathbf{x}$, while others do. This means that the last $n - r$ columns of U span the orthogonal complement of the range of A in $\mathbb{R}^n$. We thus have that the first r columns of U span the range of A. A visual sketch of the decomposition is shown in Fig.3.

We now particularize the RRQR to treat integer matrices with entries in $\{0, 1, -1\}$ and get a QR factorization such that Q and R contains entries which are still in $\{0, 1, -1\}$, further detailing the presentation given in [8]. In the considered circuit breaker, the integer matrix is the volume-to-face incidence matrix D which appears in the divergence-free constraint on the global current density $\mathbf{j}$. To this purpose, we introduce suitable terminology.

A unimodular matrix M is a square integer matrix with determinant ± 1. Equivalently, it is an integer matrix that is invertible over the integers and its inverse is again a unimodular matrix. Note that permutation matrices are unimodular as well as matrices obtained by taking products of unimodular matrices are still unimodular.

A totally unimodular (TU) matrix is a matrix for which every square non-singular submatrix is unimodular. A TU matrix is not necessarily square. Moreover, from its definition it follows that any TU matrix has only entries in the set $\{0, +1, -1\}$. We note that the incidence matrix D is TU, as every column of D contains at most two-non zero entries (since an internal face is shared by two cells and a boundary face only by one cell) and its entries are $0, +1, -1$. Moreover, it cannot happen that two non-zero entries in a column of D have the same sign since all tetrahedra in a automatically generated mesh have an outward orientation, thus, as in Fig. 2, if a face f is shared by two cells, the orientation of f agrees with that induced on it by one cell but disagrees with that induced on it by the other cell. These conditions together are sufficient for D to be a TU matrix.

For a TU matrix $A \in \mathcal{M}(\ell, q)$, we compute a unimodular matrix $\mathcal{Q}$ and a permutation matrix $\mathcal{P}$ such that

$$\mathcal{R} = \mathcal{Q}\,A\,\mathcal{P}$$

is upper triangular. As we are going to see later, the two matrices $\mathcal{Q}$ and $\mathcal{P}$ are obtained as product of a certain number of local matrices $\mathcal{Q}_{i,j}$ and $\mathcal{P}_{i,j}$ and their final goal is to put in evidence the rank deficiency of A. We use two elementary row operations to put A in reduced row echelon form:

op_1 transformation of a vector $v = (\epsilon_i, \epsilon_j)^\top$ into the vector $\tilde{v} = (1, 0)^\top$. This can be done by multiplying v on the left by the 2×2 matrix

$$\mathcal{Q}^{el}_{i,j} = \begin{pmatrix} \epsilon_i & 0 \\ -\epsilon_i & \epsilon_j \end{pmatrix}$$

thanks to the fact that, in our case, $\epsilon_i^2 = 1$.

op_2 permutation of a vector components, i.e., transformation of a vector $v = (\epsilon_i, \epsilon_j)^\top$ into the vector $\tilde{v} = (\epsilon_j, \epsilon_i)^\top$. This can be done by multiplying v on the left by the 2×2 matrix

$$\mathcal{P}^{el}_{i,j} = \begin{pmatrix} 0 & 1 \\ 1 & 0 \end{pmatrix}$$

Then, we can define

$$\mathcal{Q} = \Pi_{left}\, \mathcal{Q}_{i,j} \qquad , \qquad \mathcal{P} = \Pi_{right}\, \mathcal{P}_{i,j}$$

where the notation Π_{left} (resp., Π_{right}) indicates that the matrices $\mathcal{Q}_{i,j}$ (resp., $\mathcal{P}_{i,j}$) have to be multiplied successively on the left (resp., on the right) and

$$\mathcal{Q}_{i,j}(s,r) = \begin{cases} I(s,r) & s \neq i\,,j \quad r \neq i\,,j \\ \mathcal{Q}^{el}_{i,j}(1,1) & s = i \quad r = i \\ \mathcal{Q}^{el}_{i,j}(1,2) & s = i \quad r = j \\ \mathcal{Q}^{el}_{i,j}(2,1) & s = j \quad r = i \\ \mathcal{Q}^{el}_{i,j}(2,2) & s = j \quad r = j \end{cases}$$

The matrix $\mathcal{P}_{i,j}$ is similarly defined (just replace $\mathcal{Q}^{el}_{i,j}$ with $\mathcal{P}^{el}_{i,j}$ in the previous definition). We remark that $(\mathcal{P}^{el}_{i,j})^{-1} = \mathcal{P}^{el}_{i,j}$ due to the fact that $\mathcal{P}^{el}_{i,j}$ is a permutation matrix ($(\mathcal{P}^{el}_{i,j})^2 = I_2$). The inverse of $\mathcal{Q}^{el}_{i,j}$ is given by

$$(\mathcal{Q}^{el}_{i,j})^{-1} = \begin{pmatrix} \epsilon_i & 0 \\ \epsilon_j & \epsilon_j \end{pmatrix}.$$

Then $(\mathcal{Q}_{i,j})^{-1}$ is defined as before just replacing $\mathcal{Q}^{el}_{i,j}$ with $(\mathcal{Q}^{el}_{i,j})^{-1}$ and finally we have

$$\mathcal{Q}^{-1} = \Pi_{right}\, \mathcal{Q}^{-1}_{i,j} \qquad , \qquad \mathcal{P}^{-1} = \Pi_{left}\, \mathcal{P}^{-1}_{i,j}.$$

Now we describe the adopted procedure[1] to build up $\mathcal{Q}$ and $\mathcal{P}$ for a given TU matrix A.

function [Q,R,P]=smith(A)
Initialization step:

$$\mathcal{Q} = I_\ell \qquad , \qquad \mathcal{P} = I_q$$

per each column j with $1 \leq j \leq \min\{\ell, q\}$ do

(1) *local initialization step : $k = 0$, $i_1 = 0$, $i_2 = 0$*

[1]The two functions "smith" and "nullspace" are originally written (in pseudo-language) by the authors, they do not exist elsewhere. Their names are invented and have been chosen according to what their purpose is. The first function takes in an integer matrix (A) and gives out three integer matrices (Q, R, P such that $R = QAP$). The second one takes in an integer matrix (D) and gives out an integer matrix (N) whose columns generate the kernel of the input matrix (D).

(2) *loop on the rows i with $j \leq i \leq \ell$ to define*

$$\begin{aligned} &\mathcal{V}_j = \{ i \,|\, j \leq i \leq \ell \,,\, A(i,j) \neq 0 \} \quad , \quad k = \ \mathit{card}\ (\mathcal{V}_j) \\ &i_1 = \ \mathit{min}\ (\mathcal{V}_j) \qquad\qquad\qquad\quad , \quad i_2 = \ \mathit{min}\ (\mathcal{V}_j \setminus \{i_1\}) \end{aligned}$$

(3) *in case $k = 0$: let $\mathcal{P}_{j,z}$ be the matrix that permutes the jth column of A with the zth one. The zth column is chosen to be the first column, counted out starting from the last one, for which it exists a row index s such that $A(s,z) \neq 0$. If the index z does not exist, then stop and $\mathcal{R} = A$, otherwise do*

$$\begin{aligned} \mathcal{P} &\longleftarrow \mathcal{P}\,\mathcal{P}_{j,z} \\ A &\longleftarrow A\,\mathcal{P}_{j,z} \end{aligned}$$

and go back to step 2.

(4) *in case $k \neq 0$ but $A(j,j) = 0$ we apply a sort of partial pivot strategy : let $\mathcal{Q}_{j,i_1}$ be the matrix that permutes the jth row with the i_1th one (as explained in op_2) and do*

$$\begin{aligned} \mathcal{Q} &\longleftarrow \mathcal{Q}_{j,i_1}\,\mathcal{Q} \\ A &\longleftarrow \mathcal{Q}_{j,i_1}\,A \\ i_1 &\longleftarrow j \end{aligned}$$

and go to step 5.

(5) *in case $k \neq 0$ and $A(j,j) \neq 0$, then :*
if $k = 1$, do $j \longleftarrow j + 1$ and restart the procedure from step 1.;
if $k \geq 2$, let $\mathcal{Q}^{el}_{i_1,i_2}$ be the matrix that transforms the vector $(A(i_1,j), A(i_2,j))^\top$ into the vector $(1,0)^\top$ (as explained in op_1) and $\mathcal{Q}_{i_1,i_2}$ the associated matrix, then do

$$\begin{aligned} \mathcal{Q} &\longleftarrow \mathcal{Q}_{i_1,i_2}\,\mathcal{Q} \\ A &\longleftarrow \mathcal{Q}_{i_1,i_2}\,A \end{aligned}$$

and go back to step 1.

At the end of the procedure, the matrix A has been replaced by $\mathcal{R}$, an upper triangular one. The null space of a matrix is not affected by elementary row operations. This makes it possible to use **smith**(D) to compute N. Starting from D we thus use the procedure given below, since D has entries in the set $\{-1, 0, 1\}$.

function $[N] =$ **nullspace**(D)
Initialization step:

$$r = \mathrm{size}(D,1), \qquad s = \mathrm{size}(D,2), \qquad p = min(r,s),$$

(1) *Use elementary row operations to put D in reduced row echelon form. To this purpose run $[Q1, R1, P1] =$ **smith** (D) to get $R1$ upper triangular and run $[Q2, R^\top, P2] =$ **smith** $(R1^\top)$ to get R diagonal;*
(2) *determine rk, the rank of R, by checking how many diagonal entries of R are different from zero;*
(3) *set $n = s - rk$, where n is the dimension of the nullspace of D, and initialize N with*

$$N = \mathrm{zeros}(s,n).$$

(4) *by interpreting the reduced row echelon form as a homogeneous linear system, determine which of the variables x_1, x_2, ..., x_s are free. Write the equations for the dependent variables in terms of the free*

variables. Thus, for each free variable x_i, choose the vector for which $x_i = 1$ and the remaining free variables are zero. Then, the matrix N of size $s \times n$ is composed as follows

$$\begin{array}{lll} N(j,i) & = -R(j, rk+i), & i = 1, n, \qquad j = 1, r, \\ N(rk+i, i) & = 1, & i = 1, n \end{array}$$

(5) *apply back the two vector basis changes computed at steps (1) and (2), thus*

$$N \quad \longleftarrow \quad P1\, Q2^{\top}\, N.$$

4. The regularized LS problem

Problem (5) is solved in the least squares sense by relying on suitable factorizations of the matrix LN with real entries, as described at the beginning of section 3. If we set $A = LN$, $\mathbf{x} = \mathbf{z}$ and $\mathbf{b} = \mathbf{h}$, the least squares (LS) form of the system of equations (5) reads

$$\text{find} \quad \mathbf{z} \in \mathbb{R}^{|\mathcal{F}|-|\mathcal{C}|} \qquad \text{s.t.} \qquad ||LN\mathbf{z} - \mathbf{h}||_2^2 = \min_{\mathbf{y} \in \mathbb{R}^{|\mathcal{F}|-|\mathcal{C}|}} ||LN\mathbf{y} - \mathbf{h}||_2^2. \tag{11}$$

The numerical solution of (11) lies at the heart of many computational problems arising in scientific, engineering and economic disciplines. Efficient algorithms are available when the system matrix has full rank and is well-conditioned. However, when the matrix is ill-conditioned or rank-deficient, numerical solution of (11) often requires some variant of rank-revealing QR factorization (RRQR) or singular value decomposition (SVD). Unfortunately, the column pivoting required in the RRQR strategy does not always work for a generic real matrix. This is a very interesting but delicate subject that goes beyond the scope of the present work. Note that the modified version presented in section 3 for TU matrices does not suffer from this inconvenient. To stay on the safe side with real matrices, we solve problem (5) by using the SVD of LN. Indeed, we know that the solution to (5) is not unique as $n \leq m$. Thus, the minimum-norm solution

$$\mathbf{z} = \arg \min_{\mathbf{y} \in \mathbb{R}^n} \|LN\mathbf{y} - \mathbf{h}\|_2^2 \tag{12}$$

is sought for, that is given by $\mathbf{j} = (LN)^{\dagger}\mathbf{h}$, where $(LN)^{\dagger}$ is the pseudo-inverse of LN computed by its SVD, defined as

$$(LN)^{\dagger} = V\, \Sigma^{\dagger} U^{\top}. \tag{13}$$

4.1. Error norms

We start with a reference current density distribution $\mathbf{j}_{\text{ref}}$ to identify. then we superimpose Gaussian noise to exact synthetic data $\mathbf{h}_{\text{ref}} = L\mathbf{j}_{\text{ref}}$, and we measure the amount of noise by the signal to noise ratio r (or better, by its reciprocal, which is more suited for the present purposes). Currents $\mathbf{j}_{\text{rec},r}$ are identified by solving the inverse problem with noisy data ($\mathbf{j}_{\text{rec},0}$ is the solution to the inverse problem without noise). The original reference $\mathbf{j}_{\text{ref}}$ and reconstructed $\mathbf{j}_{\text{rec},r}$ current distributions are compared and the error $\mathbf{j}_{\text{err},r} = \mathbf{j}_{\text{rec},r} - \mathbf{j}_{\text{ref}}$ is evaluated. The magnetic field $\mathbf{h}_{\text{rec},r} = L\mathbf{j}_{\text{rec},r}$, relevant to the reconstructed currents, is computed and compared with $\mathbf{h}_{\text{ref}}$, and the error $\mathbf{h}_{\text{err},r} = \mathbf{h}_{\text{rec},r} - \mathbf{h}_{\text{ref}}$ is also evaluated.

Two merit indicators are defined, namely the relative errors on currents and magnetic fields, in the 2-norm:

$$\epsilon_{\mathbf{j}} := \frac{\|\mathbf{j}_{\text{err},r}\|_2}{\|\mathbf{j}_{\text{ref}}\|_2}, \qquad \epsilon_{\mathbf{h}} := \frac{\|\mathbf{h}_{\text{err},r}\|_2}{\|\mathbf{h}_{\text{ref}}\|_2}. \tag{14}$$

Since the goal of the method is to reconstruct currents, the most appropriate and ultimate error evaluator is a measure of the entity of $\mathbf{j}_{\text{err},r}$, i.e., $\epsilon_{\mathbf{j}}$. The error on magnetic fields and then $\epsilon_{\mathbf{h}}$ is a side-product which can be profitably used in the process of calibration of the regularization method parameters.

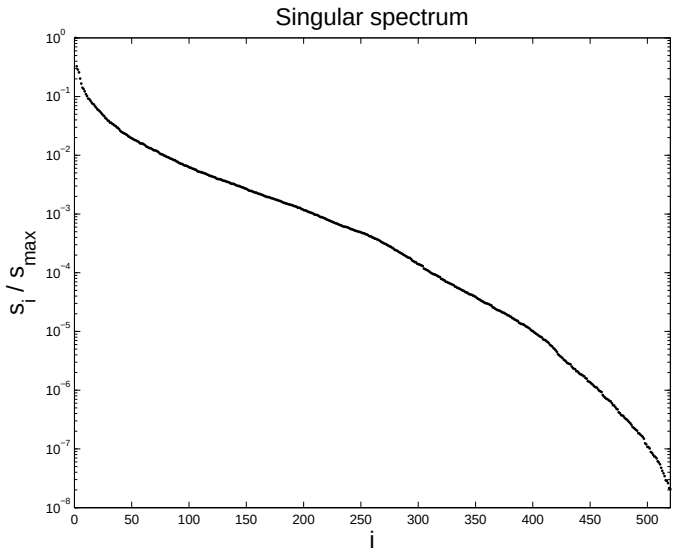

FIGURE 4. Singular value spectrum for a typical VCB case (fine approximating mesh and fine sensor array).

4.2. **Tikhonov regularization and TSVD**

A difficulty with inverse source magnetic problems is that they are notoriously ill-posed. If we consider noise as a perturbation on the magnetic field measures, the corresponding perturbation propagated to the currents is bounded by

$$\frac{\|\mathbf{j}_{\mathrm{rec},r} - \mathbf{j}_{\mathrm{rec},0}\|_2}{\|\mathbf{j}_{\mathrm{rec},0}\|_2} \leq \kappa_2 \frac{\|\mathbf{h}_{\mathrm{exp},r} - \mathbf{h}_{\mathrm{exp},0}\|_2}{\|\mathbf{h}_{\mathrm{exp},0}\|_2} \sim \kappa_2 r, \tag{15}$$

where

$$\kappa_2 := \frac{s_{\max}}{s_r} \tag{16}$$

is the condition number (in the 2-norm) of LN, that generalizes the analogous concept for standard linear systems with non singular matrices. If $\kappa_2 \gg 1$, it is possible (and virtually certain) that the unstabilized solution (12) is completely unreliable and useless. This is due to the large nullspace of LN and the consequent impossibility to block the back propagation of noise. By (16), small, non-null singular values, either intrinsic to the LN operator or of numerical error origin, yield a high condition number κ_2 (in fact, they result into large reciprocals in $\Sigma^\dagger$). Therefore they need to be filtered out in order not to possibly enhance noisy components of the measures.

A typical singular value spectrum of the problem at hand is shown in Fig. 4. The singular values are observed to decay gradually toward zero and do not show an obvious jump between zero and nonzero singular values. The condition number κ_2 remains finite, though very large. It is not infrequent that the maximum singular value be tenths of orders of magnitude bigger than the smallest non-null singular value. After [2] and [6], we refer to an inverse problem with these features as a *discrete ill-posed problem*. A typical regularization technique for such a class of problems is *Tikhonov regularization* [2], [6], arising from finding a minimizer

$$\mathbf{z} = \arg \min_{\mathbf{y} \in \mathbb{R}^{|\mathcal{F}|-|\mathcal{C}|}} \left(\|LN\mathbf{y} - \mathbf{h}\|_2^2 + \alpha^2 \|\mathbf{y}\|_2^2 \right) \tag{17}$$

instead of (12). The parameter α penalizes current distributions with a high norm, thus preventing wild fluctuations from affecting the inverse solution in order to fit the data.

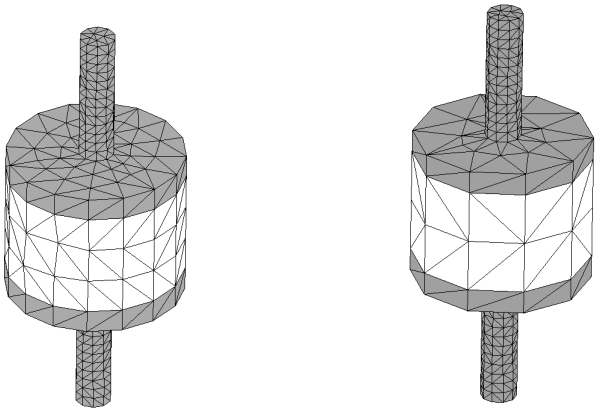

FIGURE 5. Discrete approximation of the VCB: fine mesh (left) and coarse mesh (right).

Other regularization techniques may be adopted and we use a synthetic representation for all of the most used ones. Let

$$(LN)^\sharp := VF\Sigma^\dagger U^T \tag{18}$$

be the *regularized inverse* [6], that is, the regularized counterpart of (13), where $F \in \mathrm{End}(\mathbb{R}^n)$ is a suitable filter matrix. For our needs it is sufficient to consider diagonal filter matrices of the form $F_{ij} = f_i\delta_{ij}$, where

$$f_i := \begin{cases} \dfrac{s_i^\beta}{s_i^\beta + \alpha^\beta} & \left(\text{if } \dfrac{s_i}{s_{\max}} > \delta\right) \\ 0 & (\text{otherwise}). \end{cases} \tag{19}$$

When $\delta = 0$ and $\beta = 2$, one finds Tikhonov regularization with the parameter $\alpha \ll s_{\max}$. It is immediately seen that the effect of Tikhonov regularization is to reduce the contribution of progressively smaller singular values ($s_i \ll \alpha$), for which $f_i \to 0$ and $(F\Sigma^\dagger)_{ii} = f_i/s_i \sim s_i/\alpha^2 \to 0$. When $\delta = 0$ and $\beta = 1$, one finds the *damped SVD*, similar to Tikhonov regularization but with a milder decay rate for small singular values. When $\alpha = 0$ and $\beta > 0$, one finds the *truncated singular value decomposition* (TSVD), such that all singular values below a tolerance $\delta \ll s_{\max}$ are forced to zero.

The regularized solution, replacing (12), reads

$$\mathbf{j} = N(LN)^\sharp \mathbf{h}. \tag{20}$$

It is important to notice that regularizing is not for free. As a matter of fact, with regularization schemes of the kind (19), the singular spectrum of the governing operator is altered, so that a practically unattainable precision is sacrificed, to some extent, for the sake of stability. As a consequence, the regularization scheme introduces a theoretical lower bound to the attainable accuracy.

5. Numerical examples

The current reconstruction method is tested numerically, according to what detailed hereafter. A summary of all results is reported in Table 1, where the model space (mesh, $|\mathcal{F}_p|$, $|\mathcal{C}_p|$) and data space (sensor array, $|\mathcal{P}|$) are described, along with the resulting dimensions (number of unknowns and of equations) and conditioning (κ_2) of the governing linear operator. For each case, the errors on currents ($\epsilon_{\mathbf{j}}$) and magnetic field ($\epsilon_{\mathbf{h}}$) are reported, relevant to the optimal Tikhonov penalty factor (α).

We first consider a simple case characterized by $|\mathcal{N}| = 626$ vertices, $|\mathcal{E}| = 3300$ edges, $|\mathcal{F}| = 4914$ faces and $|\mathcal{C}| = 2239$ cells. This mesh will be termed fine; see Fig. 5 (left). The inverse problem is reduced to the plasma domain only, by means of a suitable condensation technique [3], such that the metal conductors $\mathcal{T}_1$ and $\mathcal{T}_2$ are condensed onto their interface surfaces with the plasma domain $\mathcal{T}_p$. The resulting, reduced, condensed problem has now only $|\mathcal{F}_p| = 954$ faces and $|\mathcal{F}_c| = 434$ cells. The divergence free constraint is introduced through the nullspace spanning matrix N, which has dimensions 954 by 520. Therefore, 434 additional equations, corresponding to the tetrahedra in $\mathcal{T}_p$, are introduced by the divergence free constraint, lowering the number of unknowns from 954 to 520.

We use an array of 800 sensors ($3|\mathcal{P}| = 2400$), located according to a cylindrical array with 4 layers of 10 circles with 20 probes along the circumference; see Fig. 6, left. This arrangement yields an over-determined system of equations, with matrix LN which is 2400 by 520. The singular spectrum of LN is shown in Fig. 4. The minimal and maximal singular values are found to be $s_{\min} = 1.0997 \cdot 10^{-5}$ and $s_{\max} = 533.85$, respectively. The resulting condition number is thus $\kappa_2 = 4.85 \cdot 10^7$, a value that leaves no hope to approach a noisy case without regularization.

First, a noiseless condition is resolved. The procedure works very effectively, and no regularization is needed. A relative error on currents $\epsilon_{\mathbf{j}} = 0.67\%$ is found. The magnetic fields are practically exact, with a relative error $\epsilon_{\mathbf{h}} = 8 \cdot 10^{-11}$. Fig. 7 shows the current density field: reference (left), reconstructed (center) and error (right). Two ISO-magnitude surfaces are shown, partially transparent and relevant to 20% and 24% of the maximal value of current density magnitude (note that the error is not in scale with the other two). The visual effect is that of a practically perfect reconstruction of the current density field.

Then, a noisy condition with signal-to-noise ratio (SNR) 1/1% is approached. As expected, the superimposed noise on the measurements has a disruptive effect on the ill-conditioning of the LN operator. We try to heal the inverse problem solution by means of Tikhonov regularization, obtaining the trends shown in Fig. 8, where in the left picture the relative errors on currents (bold line) and magnetic fields (thin line) are drawn Vs. the α penalty factor (adimensionalized by the greatest singular value). As α is increased, a steep descent is observed in the error on currents, from hyperbolic values down to $\epsilon_{\mathbf{j}} = 58.00\%$. The right picture is a parametric plot originated by the two relative errors, taking α as a parameter, and shows that the best compromise is found in the bend of the typical L shaped curve. Consequently, the error on magnetic fields is still low, and precisely $\epsilon_{\mathbf{h}} = 0.28\%$. Unfortunately, the error on currents, even in the best case, is useless for engineering purposes, and some finer approach is needed. Fig. 9 shows the current density field, under the same assumptions already discussed in the exact case.

We tested the method also with the sensor arrays shown in Fig. 6 (center and right) and characterized by, respectively, only 2 and 1 layers, instead of 4. The good quality of the exact case solution is preserved, as well

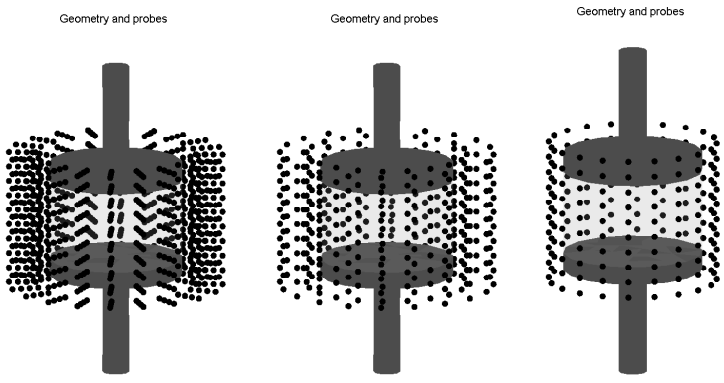

FIGURE 6. Array of sensors located around the VCB under test: fine (left), medium (center), coarse (right).

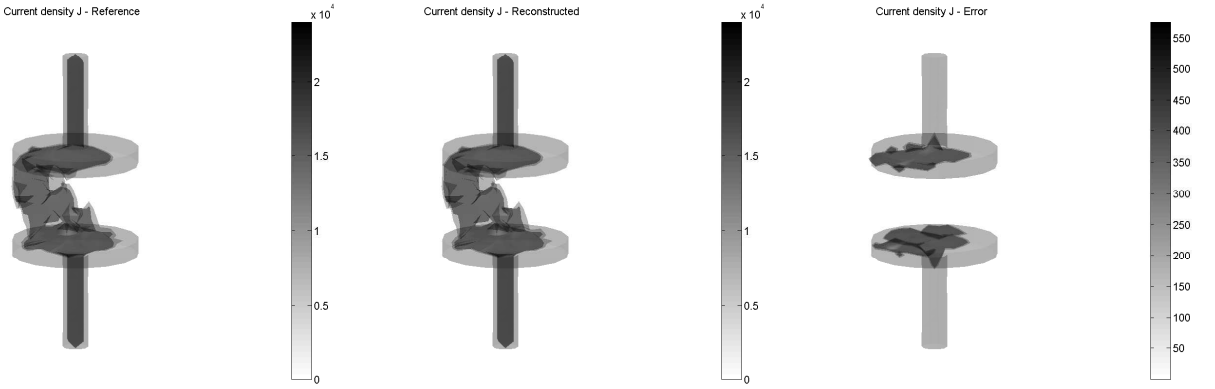

FIGURE 7. Current density field in a noiseless case, with a fine mesh and fine sensor array: reference (left), reconstructed (center) and error (right).

as the trends and values observed in the regularization of the noisy case. Similar results (not reported) are obtained by means of the TSVD regularization scheme.

Since the problem with inverse identification is its ill-conditioning, and since the condition number increases with the size of the problem, the current reconstruction method is also tested on a coarser mesh, characterized by $|\mathcal{N}| = 497$ vertices, $|\mathcal{E}| = 2567$ edges, $|\mathcal{F}| = 3786$ faces and $|\mathcal{C}| = 1715$ cells. This mesh will be termed coarse; see Fig. 5 (right). When reduced to the plasma domain only, the resulting, condensed problem has now only $|\mathcal{F}_p| = 300$ faces and $|\mathcal{C}_p| = 132$ cells. The divergence free constraint is introduced through the nullspace spanning matrix N, which has dimensions 300 by 168. Therefore, 132 additional equations, corresponding to the tetrahedra in $\mathcal{T}_p$, are introduced by the divergence free constraint, lowering the number of unknowns from 300 to 168.

The fine sensor array is still used; see Fig. 6, left. This arrangement yields an over-determined system of equations, with matrix LN which is 2400 by 168. The minimal and maximal singular values are found to be

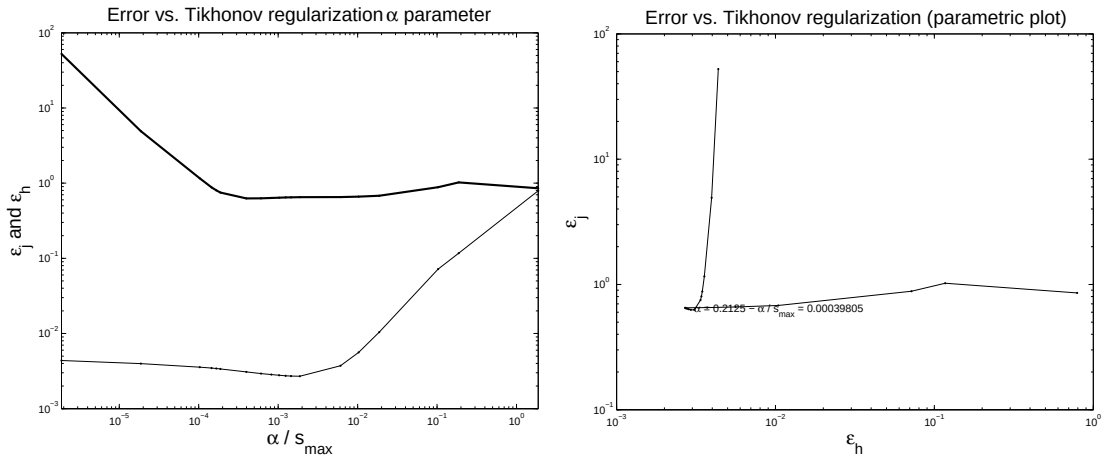

FIGURE 8. Tikhonov regularization in a noisy case (SNR=1/1%), with a fine mesh and fine sensor array. Left picture: error on currents (bold line) and on magnetic field (thin line) Vs. α penalty factor (adimensionalized with the greatest singular value). Right picture: parametric plot of the errors on currents and magnetic field, with the typical L shape.

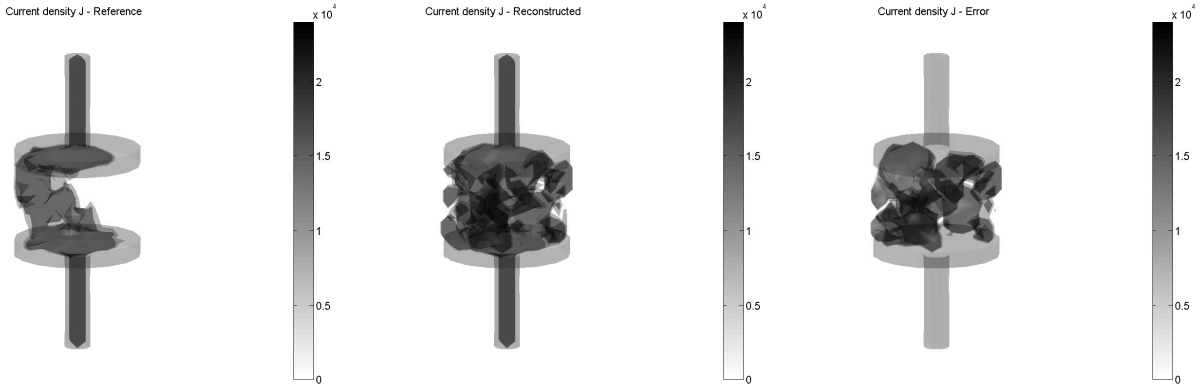

FIGURE 9. Current density field in a noisy case (SNR=1/1%), with a fine mesh and fine sensor array: reference (left), reconstructed (center) and error (right).

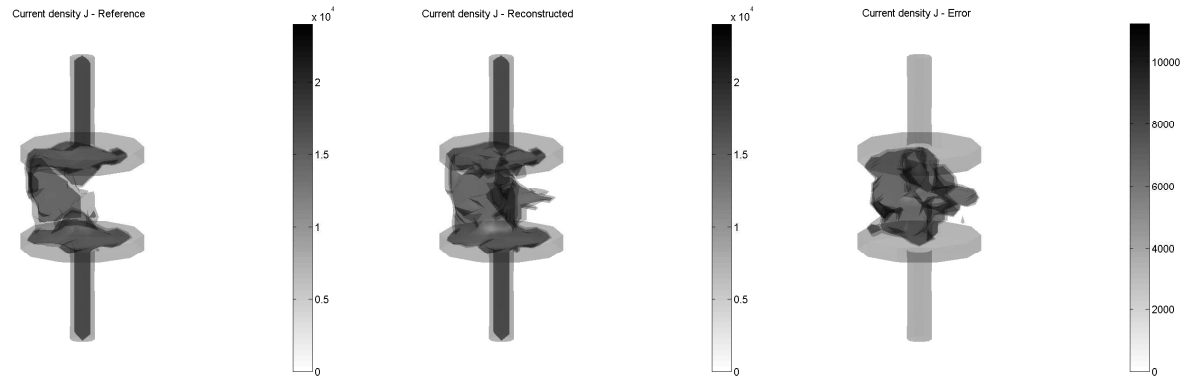

FIGURE 10. Current density field in a noisy case (SNR=1/1%), with a coarse mesh and fine sensor array: reference (left), reconstructed (center) and error (right).

$s_{\min} = 7.2727 \cdot 10^{-3}$ and $s_{\max} = 311.79$, respectively. The resulting condition number is thus $\kappa_2 = 4.29 \cdot 10^4$, which is three orders of magnitude lower than in the fine mesh case.

The noisy condition with signal-to-noise ratio (SNR) 1/1% is solved. A similar exploration method is used to get the optimal α penalty factor. Correspondingly, the error on currents has decreased down to $\epsilon_{\mathbf{j}} = 19.74\%$, and the error on magnetic fields is always low, and precisely $\epsilon_{\mathbf{h}} = 0.23\%$. Fig. 10 shows the current density field, under the same assumptions already discussed. Although the error on currents is better but still useless for engineering purposes, this test shows a clear trend (expected from the theory of inverse problems) and suggests trying to adopt a multi-scale approach, starting with a coarse mesh and later refining the result with finer grids. Well assessed regularization techniques exist, based on Tikhonov method, in order to penalize strong deviations from a former, coarser estimate of the solution; see, e.g., [6]. This idea is not developed in the present study.

6. Concluding remarks

Circuit breakers constitute an important (environmentally speaking), world-wide, rich business and their study lies at the heart of the researches done by the R&D Labs of all industries in charge of electrical systems design and power generation. Note that we do not have in general free access to their obtained results as they are confidential. Some of the manufacturers are ABB, GE (General Electric) , Tavrida Electric, Alstom, Mitsubishi

Mesh	Sensor array	$\lvert\mathcal{F}_p\rvert$	$\lvert\mathcal{C}_p\rvert$	$\lvert\mathcal{P}\rvert$	Unknowns	Equations	κ_2	$\epsilon_{\mathbf{j}}$	$\epsilon_{\mathbf{h}}$	α
fine	fine	954	434	800	520	2400	$4.85 \cdot 10^7$	58.00%	0.28%	0.3250
	medium			400		1200	$5.16 \cdot 10^7$	66.37%	0.47%	3.2500
	coarse			200		600	$7.22 \cdot 10^7$	62.23%	0.60%	0.3250
coarse	fine	300	132	800	168	2400	$4.29 \cdot 10^4$	19.74%	0.23%	0.2125
	medium			400		1200	$3.30 \cdot 10^4$	22.72%	0.33%	0.2125
	coarse			200		600	$2.78 \cdot 10^4$	25.27%	0.45%	0.3250

TABLE 1. Summary of numerical results: all cases with signal-to-noise ratio = 1/1% (noiseless case are solved practically exactly).

Electric, Pennsylvania Breaker, Siemens, Toshiba, Koncar HVS, BHEL, CGL, Square D (Schneider Electric). We have led a preliminary (simple and numerical) study of the current identification in vacuum circuit breakers. From the analyzes carried out it follows that it is numerically feasible to reconstruct the electric currents in the plasma phase inside a high voltage, vacuum circuit breaker by inverting magnetic field data. The presented results can however be improved by relying on other more sophisticated regularization techniques as well as by analyzing other ways to construct the Biot-Savart-like operator L, involving for example suitable (Whitney) elements [1] for the current and the magnetic field.

REFERENCES

[1] A. BOSSAVIT, *Computational Electromagnetism*. Academic Press, New York (1998).

[2] R.C. ASTER, B. BORCHERS, C.H. THURBER, *Parameter Estimation and Inverse Problems*, Elsevier Academic Press (2005).

[3] L. GHEZZI, A. BALESTRERO, *Modeling and Simulation of Low Voltage Arcs*, Ph.D. Dissertation, Technische Universiteit Delft (2010).

[4] L. GHEZZI, D. PIVA, L. DI RIENZO, *Current Density Reconstruction in Vacuum Circuit Breakers by Inverting Magnetic Field Data*, IEEE Transactions on Magnetics, under review.

[5] G.H. GOLUB, C.F. VAN LOAN, *Matrix computations*, The Johns Hopkins University Press, Maryland (1985).

[6] P.C. HANSEN. *Rank-Deficient and Discrete Ill-Posed Problems, Numerical Aspects of Linear Inversion.* Society for Industrial and Applied Mathematics (1998).

[7] J.W. MCBRIDE, A. BALESTRERO, L. GHEZZI, G. TRIBULATO, K.J. CROSS. Optical fiber imaging for high speed plasma motion diagnostics: Applied to low voltage circuit breakers, *AIP Rev. Sci. Instr.*, 81(5) (2010).

[8] F. RAPETTI, F. DUBOIS, A. BOSSAVIT, *Discrete vector potentials for non-simply connected three-dimensional domains*, SIAM J. on Numerical Analysis, 41(4) (2003), pp. 1505-1527.

[9] H.J.S. SMITH, *On systems of linear indeterminate linear equations*, Phil. Trans., 151 (1861), pp. 293-326.